

LHCb 2010 luminosity determination with van der Meer scans

V. Balagura, CERN, Geneva, Switzerland & ITEP, Moscow, Russia

Abstract

The absolute calibration of LHCb 2010 luminosity performed with van der Meer scans is discussed.

INTRODUCTION

The luminosity in LHCb is constantly monitored with randomly triggered at 1 kHz events. They are usually called “nano-events” because they contain only an information relevant for the luminosity measurement and everything else is stripped off. The load on LHCb data acquisition system is therefore almost negligible. This approach of luminosity monitoring was proposed in [1]. “Nano-events” contain so called “luminosity counters”, i.e. quantities proportional to the luminosity and easily measurable online. In 2010 we used as counters a number of vertexes, tracks and hits in a vertex detector (VELO), a number of hits in a scintillator pad detector (SPD) in front of calorimeters, and a transverse energy deposition in the calorimeters.

The relative luminosity can be determined from the average value of any counter. Alternatively one may determine it from the fraction of empty events with the counter close to zero, which we denote by $P(0)$. The luminosity should be proportional to $-\log P(0)$. This is obvious for the Poisson distribution, but in fact is also valid generally. Indeed, let’s suppose that the counter x can not take negative values. Suppose, there are two independent sources contributing to x and they individually give spectra P_1 and P_2 . The resulting spectrum is a convolution $P = P_1 \otimes P_2$. Since both sources can not produce negative x , a zero sum means zero contributions from P_1 and P_2 , so that $P(0) = P_1(0) \cdot P_2(0)$ and $\log P(0) = \log P_1(0) + \log P_2(0)$. Therefore $\log P(0)$ is an additive quantity which should be proportional to the luminosity. This also implies that in the presence of backgrounds its contribution $-\log P_{\text{bgr}}(0)$ may be subtracted. Note, that the background distribution should not necessarily follow Poisson law. $-\log P_{\text{bgr}}(0)$ is estimated in LHCb from the crossings where one bunch is filled and the other is empty. In the crossings with pp -collisions it is renormalized assuming that the dominating beam-gas background is proportional to the beam currents.

We define an “empty” event as having $x \leq x_0$ with some threshold x_0 . The above arguments hold only for $x_0 = 0$ since we assumed that $x = x_1 + x_2 = 0$ implies $x_1 = x_2 = 0$. If $x_0 > 0$, some systematic error appears. To avoid it, one may use the average value of the counter $\langle x \rangle$ instead of $-\log P(0)$. In this case another systematics may appear however, if the counter is not exactly proportional to the luminosity. The discussion of

both methods and their comparison with the luminosity estimation from the fit of the x spectrum, which is the most precise procedure, is discussed in [2]. In particular, it explains how the x spectrum can be conveniently described using Fourier transforms.

During commissioning in 2010 several modifications have been made in LHCb subdetectors influencing luminosity counters. We chose the number of tracks reconstructed in VELO in R - Z projection as the best and the most stable counter. We used $-\log P(0)$ method for it and defined an “empty” event as having zero or one track. The systematics associated with this choice of threshold is negligible since the average interaction produces ~ 30 tracks. Modifications and alignment variations of VELO also produced almost negligible impact on the method, since the efficiency of reconstruction of at least two tracks in an inelastic event was always close to 100%. The stability of the counter is demonstrated in Fig. 1 which shows the ratio of the relative luminosities determined with $-\log P(0)$ method from the multiplicity of hits in the upmost layer of VELO and from the number of R - Z tracks. The former was also stable throughout LHCb 2010 running, and we used it as a cross check. Fig. 1 covers the whole period of LHCb operation, with both low and high number of interactions per crossing. Two counters have different systematics, and by comparing them we assign a systematic error of 0.5% to the relative luminosity measurement.

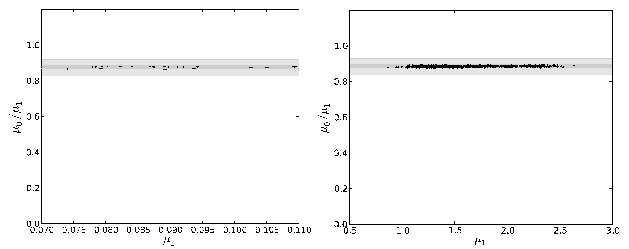


Figure 1: Ratio of average numbers of interactions per crossing μ_{PU}/μ_{RZ} determined with $-\log P(0)$ method from the number of hits in the upmost (so called pile-up or PU) layer of VELO and the number of R - Z tracks, versus μ_{RZ} . The deviation from unity is due to the difference in acceptance. Left (right) plot is for the beginning (the end) of LHCb 2010 running with lower (higher) values of μ .

The absolute calibration of LHCb luminosity was performed in 2010 using a beam-gas imaging method and van der Meer scans. In the former the images of two beams were developed from their interactions with a small amount of gas remaining in the beam pipe, assuming the uniform

gas distribution across the beams. The luminosity was calculated from the beam overlap integral obtained from the beam images. The method was proposed in [3] and first applied in LHCb in [4, 5]. At this workshop it was discussed in [6]. Here we concentrate on the alternative absolute luminosity calibration proposed by van der Meer [7].

The calibrations obtained with two methods were consistent and were averaged for the final result. The methods had similar sensitivity limited in 2010 by uncertainties in beam intensities. Other systematic errors were different, therefore usage of both in LHCb provided an important cross check of the results.

VAN DER MEER SCAN EXPERIMENTAL CONDITIONS

Van der Meer scans in LHCb have been performed in the dedicated LHC fills in the beginning and in the end of 2010 running, in April and in October. The characteristics of the beams are summarized in Table 1. In both fills there were two scans where either both beams moved symmetrically or only one at a time. Beam movements recorded with LHC Beam Position Monitors (BPMs) up- and downstream of LHCb are shown in Fig. 2. Note, that for the following analysis we did not use this information since BPM measurements were temperature dependent and were drifting with time. Precise beam positions were calculated from LHC magnet currents and cross checked with LHCb VELO detector, see later.

Table 1: Parameters of LHCb van der Meer scans. $I_{1,2}$ is a typical number of protons per bunch in units 10^{10} , n_{all} (n_{coll}) is the total number of bunches per beam (number of colliding bunches), μ_{max} is the maximal average number of interactions per crossing, $\tau_{I_1 \times I_2}$ and τ_L are the decay times of the bunch intensity product and of the luminosity, respectively, in hours.

	25 Apr	15 Oct
LHC fill	1059	1422
$I_{1,2}$	1	7-8
β^*	2	3.5
$n_{\text{coll}}/n_{\text{all}}$	1/2	12/16
μ_{max}	0.03	1
trigger	min.bias	22.5 kHz random <1 kHz min.bias beam-gas
$\tau_{I_1 \times I_2}$	950	700
τ_L	30	46

In April the maximal beam separation was achieved only in the first scan, as in the second only the first beam was allowed to move. In October, in the second scan both beams moved one after the other. This allowed to cover the whole separation range. However, the beam steering procedure was such that in the middle of the scan the first beam jumped to an opposite end point and then returned back, so

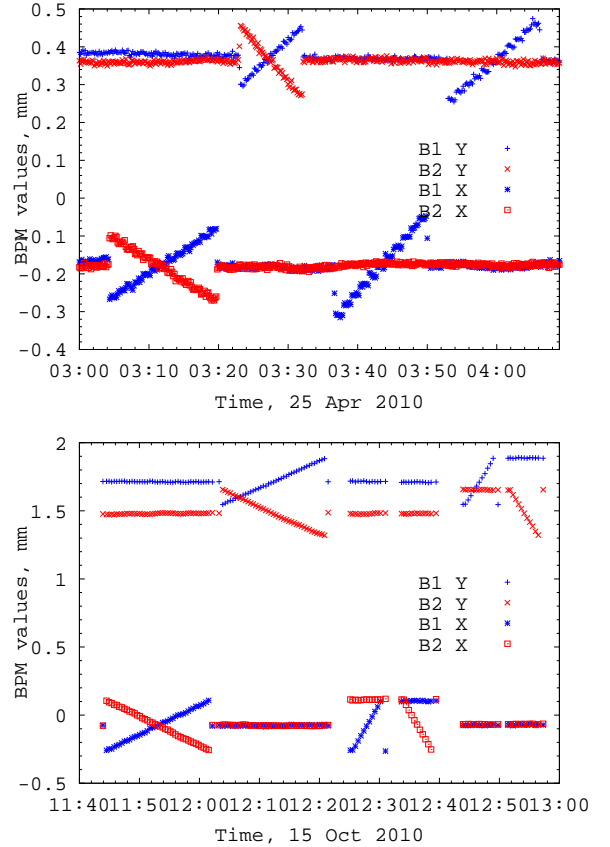


Figure 2: Beam movements recorded with LHC Beam Position Monitors (BPMs) around LHCb point in April (top) and in October (bottom). The zero points on the vertical axes are arbitrary. Top (bottom) curves show time dependent coordinates of two beams, $y_{1,2}$ ($x_{1,2}$). In both LHC fills there were two scans, first in $\Delta x = x_1 - x_2$ and then in $\Delta y = y_1 - y_2$. In the first scan both beams moved symmetrically, in the second scan either only the first beam was moved (April) or the first in the beginning and the second in the end (October).

that the beam movement was not continuous. This could potentially increase hysteresis effects in the LHC magnets. In addition, second scan in October had twice less data points, so we used it only as a cross check to estimate systematic errors.

In April the event rate was low and it was possible to record all events with pp interactions. We used loose minimum bias trigger with the minimal requirements on number of SPD hits (≥ 3) and transverse energy deposition in the calorimeters (≥ 240 MeV). In October the bunch intensities were higher by ~ 7.5 , therefore in spite of slightly broader beams ($\beta^*=3.5$ instead of 2), the rate was significantly larger, by a factor of ~ 30 . In addition, there were 12 colliding bunches instead of one in April. Therefore we used selective trigger with three lines running in parallel. The first line accepted random “nano-events” at 22.5 kHz (20 kHz were devoted to 12 crossings with colli-

sions, 1 + 1 kHz - to 4 + 4 crossings where only one of two beams was present, and 0.5 kHz to all other empty crossings). The second line was the same loose minimum bias trigger but rate limited at 1 kHz. The third line collected events for the beam-gas analysis.

Both in April and in October the systematic error was dominated by uncertainties in the beam intensities. In April it was higher (5.6%) because of larger contribution from the offset uncertainty at lower beam intensities [8]. In October the calibration factor in the intensity measurement (2.7%) became dominant [9]. Both scans gave consistent results, and in the following we concentrate on the later scan with about twice better precision.

Time stability

Beam intensities in LHC are measured with Direct Current (DC) and Fast Beam-to-Current Transformers (BCTs) [10]. The former provides ultimate precision for the total current in the ring, while the latter gives information on relative bunch populations. Fig. 3 shows the DC BCT beam intensities before, during and after van der Meer scan fill in October. Fig. 4 presents the relative evolution of the individual bunch charges during LHCb scans. The LHC filling scheme was chosen in such a way that all bunches were collided only in one (or two for ATLAS/CMS) experiment, namely 12 in LHCb, 3 in ATLAS/CMS and 1 in ALICE. It is interesting that LHCb bunches demonstrated the best time stability. They changed during two LHCb scans by less than 0.1%. Therefore we did not normalize the rates by the intensity product $I_1 \times I_2$ at every scan point, but instead used only one average product per scan. This was done to avoid the noise associated with $I_{1,2}$ measurement. The averaged bunch intensities are given in Table 2. The same procedure was applied for the April scan, when the decay time of $I_{1,2}$ was even longer, 950 instead of 700 hours in October.

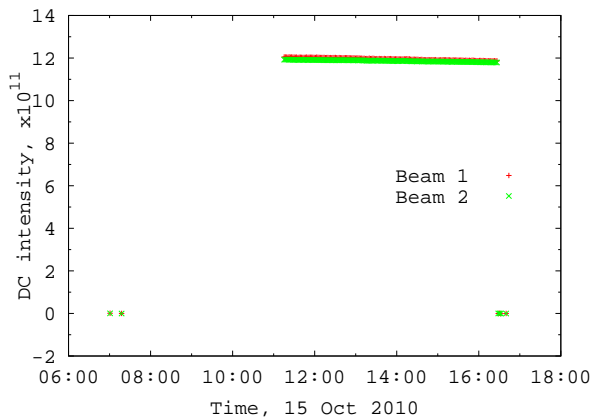


Figure 3: Intensities of two beams measured with DC BCT (system A) before, during and after van der Meer scan fill in October.

In addition to the beam intensity changes the luminosity stability may be limited by the changes in the bunch pro-

Table 2: Beam intensities averaged over two scan periods. The bottom line is DC BCT measurement, everything else is Fast BCT. The first 12 rows are the measurements in bunch crossings (BX) with collisions at LHCb, and the last two lines are the sums over all 16 bunches.

BX	Scan 1		Scan 2	
	I_1	I_2	I_1	I_2
2027	8.425	7.954	8.421	7.951
2077	7.949	7.959	7.944	7.957
2127	7.457	7.563	7.452	7.561
2177	6.589	7.024	6.584	7.021
2237	7.315	8.257	7.311	8.255
2287	7.451	7.280	7.446	7.278
2337	7.016	7.219	7.012	7.217
2387	7.803	6.808	7.798	6.805
2447	7.585	7.744	7.580	7.742
2497	7.878	7.747	7.874	7.745
2547	6.960	6.244	6.955	6.243
2597	7.476	7.411	7.472	7.409
All, Fast	120.32	119.07	120.18	118.99
DC	120.26	119.08	120.10	118.98

files, e.g. by an emittance growth. The luminosity stability was checked several times during the scans when the beams were brought to their nominal positions. The measured luminosities are shown in Fig. 5 for the October scan. The luminosity decay time was measured to be 46 hours (30 hours in April). This corresponds to 0.7% luminosity drop during the first (longer) scan along either Δx or Δy (0.9% in April). As it will be discussed later, in van der Meer method one needs the integrals of the luminosity over the separations Δx and Δy . The scan points have been taken from lower to higher Δx , Δy values, therefore the luminosity drop effectively enhances slightly the left part of the integral and reduces its right part, so that the net effect to the first order cancels, since the curve is symmetric. The luminosity at the nominal beam positions also entering van der Meer formula, was measured in the beginning, the middle and the end of every scan, so that the luminosity drop also cancels to the first order. Therefore the systematic error due to the luminosity drop was much less than 0.7% and was neglected.

Fig. 6 shows the luminous region profiles when the beams were brought to their nominal positions during the first and the second scans in Δx and Δy . One can see that the widths did not change within the statistical errors which also presents an evidence of the negligible emittance growth. In addition, in the following it will be demonstrated that the widths of van der Meer plots with the luminosity dependence on Δx , Δy are also stable.

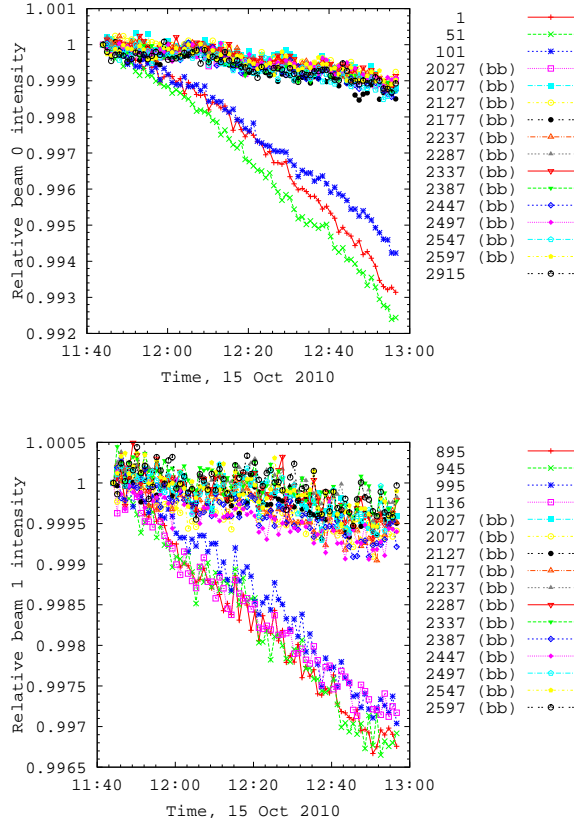


Figure 4: Relative evolution of the individual bunch charges measured with Fast BCT (system A) during two LHCb scans in October. Top (bottom) plot corresponds to the first (second) beam. Three (four) bunches in the bottom with faster decay time collided in ATLAS/CMS (or in ALICE).

CROSS SECTION DETERMINATION

In case of x - y factorization the cross section can be determined from Δx , Δy scans with van der Meer formula

$$\sigma = \frac{\int \mu(\Delta x, \Delta y_0) d\Delta x \times \int \mu(\Delta x_0, \Delta y) d\Delta y}{N_1 N_2 \mu(\Delta x_0, \Delta y_0) \cos \alpha}, \quad (1)$$

where $N_{1,2}$ are the bunch intensities, μ is the average number of interactions per crossing and α is a half of the beams crossing angle (270 and 170 μ rad in April and in October, respectively). It is assumed that protons in the beams move with the speed of light. $(\Delta x_0, \Delta y_0)$ is the crossing point where the beams return to their nominal positions, which is not necessarily the point of the maximal luminosity. The derivation of this formula is given in [11]. The interaction definitions for μ and for σ should be the same, but otherwise are arbitrary. We defined it as a pp interaction with ≥ 2 VELO tracks in R - Z projection, in accordance with the definition of our best luminosity counter.

12 bunches collided in October were analysed individually. The separation Δx , Δy dependence of μ averaged over all bunches is shown in Fig. 7. Two scans are over-

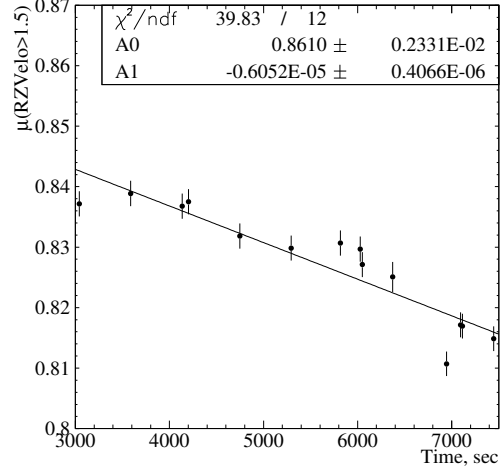


Figure 5: The evolution of the average number of interactions per crossing at the nominal beam positions during October scans. In the first (second) scan both in Δx and Δy the nominal point parameters were measured three (four) times. The line is a fit to the first order polynomial, the fit parameters are given in the top right corner. The luminosity decay time is $1/0.605 \cdot 10^{-5}$ sec = 46 hours.

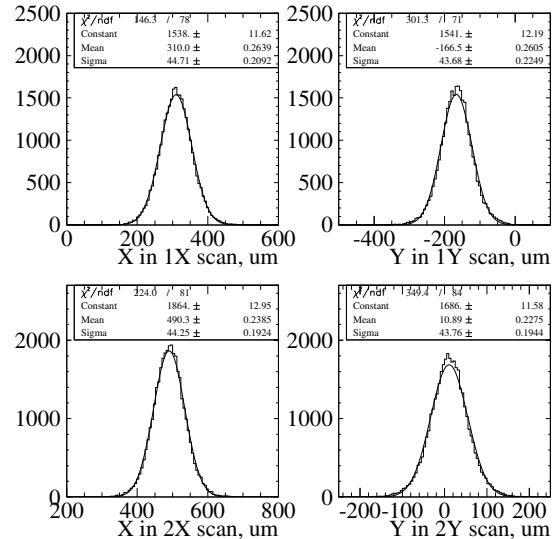


Figure 6: The luminous region profiles measured with the beams at their nominal positions during the first and the second scan in October in Δx and Δy . 12 colliding bunches are combined. The curve is a Gaussian fit with the parameters listed in the top right corner.

laid, the second was taken at the same points but with twice larger step. One can see that its Δy curve is shifted from the first scan by $7 \mu\text{m}$ on the left and by $4 \mu\text{m}$ on the right side. The reason of non-reproducibility is not understood. It may be attributed to the hysteresis effects enhanced in the second scan.

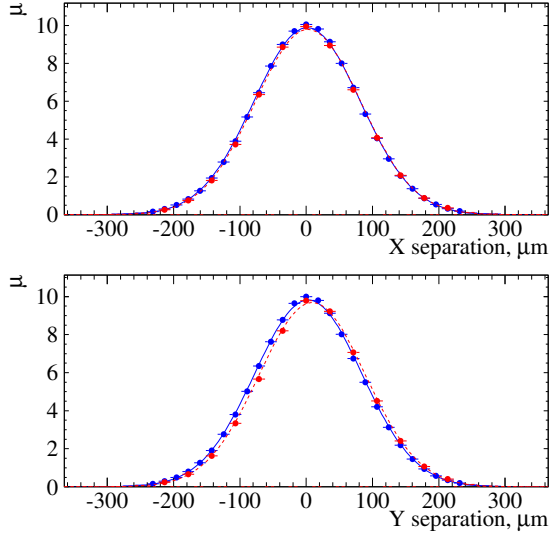


Figure 7: Averaged over 12 bunches number of interactions per crossing versus the separations Δx , Δy in October. The first (second) scan is represented by blue (red) points and solid (dashed) lines.

Similar curves for the April scans are shown in Fig. 8 where some shift in Δx is present.

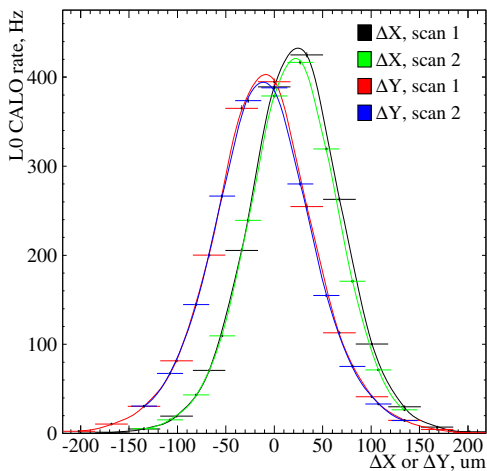


Figure 8: Trigger rate in April scan corrected for a small probability of multiple interactions and thus proportional to the luminosity versus the beam separations Δx , Δy . First and second scans are overlaid.

The curves were fit to single and double Gaussian. The results of the former for the October scans together with the mean and RMS values are listed in Table 3. There is no evidence for the emittance growth as the widths in two scans were the same within the errors.

Table 3: Mean, RMS and single Gaussian fit results for the October scans averaged over 12 bunches.

	Δx scan	Δy scan
mean	1.29 2.79	3.10 9.16
RMS	80.56 80.49	80.82 80.71
χ^2/ndf	1881 / 38 1362 / 18	827 / 38 819 / 18
constant	9.880 ± 0.008 9.789 ± 0.010	9.820 ± 0.008 9.681 ± 0.009
center	1.30 ± 0.05 2.77 ± 0.07	3.10 ± 0.05 9.11 ± 0.07
sigma	80.25 ± 0.04 79.95 ± 0.05	80.73 ± 0.04 80.35 ± 0.05

Double Gaussian fit gives a much better description. We fit all bunches individually, Fig. 9 gives one example for the first two bunches in October. The Δy curve is shifted from zero to the right for illustration purposes to be distinguished from Δx . It was found that the fit errors can be reduced approximately by half if the fit of Δx and Δy curves was performed simultaneously and the value at the nominal point $\mu(\Delta x_0, \Delta y_0)$ was constrained to be the same in both scans. The first fit parameter was chosen to be $\int \mu d\Delta x \cdot \int \mu d\Delta y / \mu(\Delta x_0, \Delta y_0)$, the term appearing in Eq. (1), so that a cross correlation of both integrals and the value at the nominal point is correctly taken into account in the resulting fit error. Other fit parameters listed in Fig. 9 are: two integrals along Δx and Δy , σ_1 , $\Delta\sigma$ and a common Gaussian center for Δx and then for Δy curves. Here σ_1 is the width of the first Gaussian, while $\sigma_2 = \sqrt{\sigma_1^2 + \Delta\sigma^2}$, ensuring $\sigma_2 > \sigma_1$. Relative normalization of two Gaussians and the value at the nominal point were derived from nine fit parameters listed above. χ^2/ndf for all bunches was always between 0.7 and 1.8.

The product of bunch intensities $I_1 \cdot I_2$ in 12 colliding bunches is shown in Fig. 10. In spite of RMS spread of 12%, the bunches give cross sections consistent within statistical errors, having an average of 0.29% in the first scan. The sensitivity of the method is so high that we decided to use it to cross calibrate the *relative* bunch populations $I_{1,2}^i / \sum_{j=1}^{16} I_{1,2}^j$ measured with Fast BCT system. Here i runs over 12 LHCb bunches. By comparing Fast BCT with ATLAS BPTX measurements it was observed, that both may have a non-zero offset, see [8], [9]. Therefore we fit our 12 cross section measurements with three parameters: common cross section σ and Fast BCT offsets for two beams $I_{1,2}^0$. The offset uncorrected cross sections

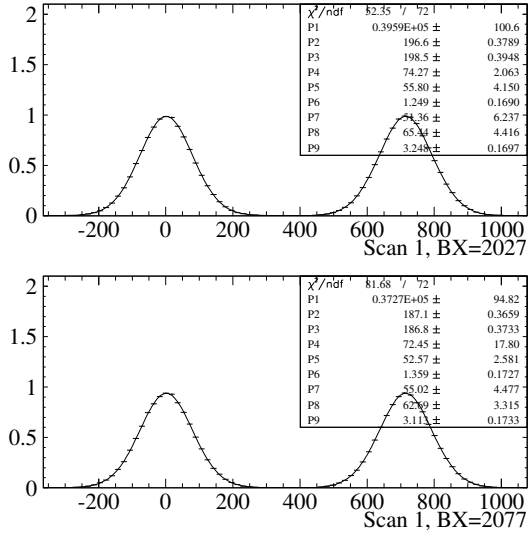


Figure 9: Number of interactions per crossing μ versus the separations Δx , Δy for the first two colliding bunches in the first October scan. Δx and Δy curves are stacked one after the other for illustration purposes. Fitting curves and parameters are discussed in the text.

are shown in Fig. 11. They are fit to the function

$$\sigma \cdot \prod_{b=1,2} (I_b^i - I_b^0) / I_b^i \cdot \sum_{k=1}^{16} I_b^k / \sum_{j=1}^{16} (I_b^j - 16 \cdot I_b^0)$$

which uses Fast BCT offset corrected relative populations and implies DC BCT $I_{1,2}^{DC}$ total beam intensities. Two offsets improve the description of the points compared to the uncorrected simple fit by a constant. The latter has a goodness of fit probability of 1.5% and 2.5% in two scans, or $2.3 \cdot 10^{-3}$ if they are combined. The χ^2/ndf and all other fit results are summarized in Table 4, which also contains a section when ATLAS BPTX was used instead of Fast BCT system.

One can see that the offset errors in the first scan are $(0.10 - 0.12) \cdot 10^{10}$, or 1.5% relative to the average bunch intensity $\langle I_{1,2} \rangle = 7.5 \cdot 10^{10}$. The sensitivity of the method, therefore, is very high, in spite of the fact that the RMS spread of intensities $I_1 \cdot I_2$ was only 12%. It may be very advantageous to make bunches in the future scans as different as possible, to become even more sensitive to the offsets and also to probe other effects like beam-beam interactions which may be visible at high but not at low intensities.

The offset and cross section errors are only statistical. Since the fits return good χ^2/ndf values, the bunch crossing dependent systematics should be at a lower or at a comparable level. The relative cross section error is only 0.09%, although the cross section difference between Fast BCT and BPTX fits is twice larger. One can also see that the BPTX offset I_2^0 for the second beam differs in two scans by 1.6σ .

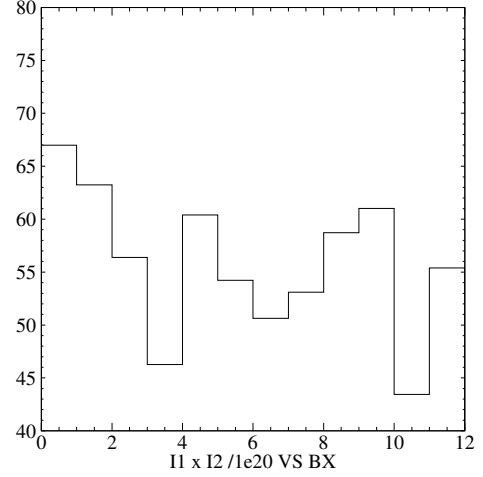


Figure 10: Bunch intensity products $I_1 \cdot I_2$ for 12 colliding bunches in October.

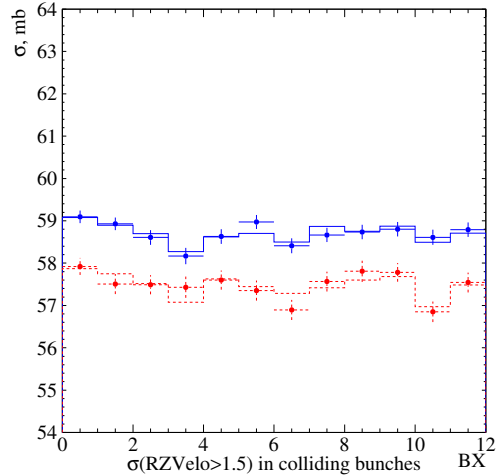


Figure 11: Cross sections not corrected for Fast BCT offset for 12 LHCb bunches in October. The upper (lower) curve is obtained in the first (second) scan. The fit takes into account Fast BCT offset and is discussed in the text. The fit results are summarized in Table 4.

This gives the level of systematic errors. All main sources of systematics which will be discussed later (DC BCT uncertainty, hysteresis, ghost charges etc.) cancel when comparing bunches.

In spite of a good agreement between the bunches within the same scan, there is an overall 2.1% discrepancy between the scans. The reason is not understood, and may be attributed to the potential hysteresis or similar effects resulting to uncontrollable shifts of the beam as a whole. We took the results of the first scan with Fast BCT offsets for the final LHCb luminosity determination. 2.1% is the second largest systematic error in the cross section measure-

Table 4: Results of the cross section fit over 12 LHCb bunches in October. $I_{1,2}^0$ are Fast BCT or BPTX offsets in units 10^{10} . They should be subtracted from the values measured for individual bunches. Last two columns are for the first and the second scan, respectively. The cross section from the first scan obtained with Fast BCT intensities with offsets is used for LHCb luminosity calibration.

Fast BCT		
σ , mb	58.73 ± 0.05	57.50 ± 0.07
I_1^0	0.40 ± 0.10	0.29 ± 0.15
I_2^0	-0.02 ± 0.10	0.23 ± 0.13
χ^2/ndf	5.8 / 9	7.6 / 9
with zero offsets		
σ , mb	58.73 ± 0.05	57.50 ± 0.07
χ^2/ndf	23.5 / 11	21.9 / 11
ATLAS BPTX		
σ , mb	58.62 ± 0.05	57.45 ± 0.07
I_1^0	-0.10 ± 0.12	-0.23 ± 0.17
I_2^0	-0.63 ± 0.12	-0.34 ± 0.15
χ^2/ndf	6.9 / 9	7.3 / 9
with zero offsets		
σ , mb	58.63 ± 0.05	57.46 ± 0.07
χ^2/ndf	66.5 / 11	23.5 / 11

ment after uncertainties in the beam intensities. If DC BCT accuracy will improve in future 2011 scans, this may become a dominating error. In April the situation was similar, the discrepancy was $(4.4 \pm 1.2)\%$, the results may be found in Table 5. Since the April measurement was performed with the trigger rates proportional to the luminosity, instead of R - Z VELO tracks, we corrected the results for the difference in acceptances $\sigma(RZ)/\sigma(\text{April trigger}) = 1.066$. At that time Δx and Δy curves were fit separately. To obtain the average number of interactions from the trigger rates we used LHC revolution frequency 11.245 kHz.

Table 5: Cross section results in April. R is the trigger rate corrected for the small probability of multiple interactions and thus proportional to the luminosity. $\sigma(RZ)$ is the cross section of the interaction with ≥ 2 R - Z VELO tracks.

	Scan 1	Scan 2
$\int R d\Delta x$, cm·Hz	5.107 ± 0.017	4.875 ± 0.016
$\int R d\Delta y$, cm·Hz	5.094 ± 0.025	4.994 ± 0.016
$R(\Delta x_0, \Delta y_0)$, Hz	392	383
$I_1 \cdot I_2, \times 10^{10}$	1.056	1.056
$\sigma(RZ)$	59.6	57.0

SYSTEMATIC ERRORS

Δx and Δy length scale

Δx and Δy beam separation values at every scan step are calculated from the LHC magnet currents. There was a small non-reproducibility in the results of two scans, as it may be seen from Figs. 7 and 8, which may be attributed to the mismatch of the beam positions. Therefore it is important to check Δx and Δy values, and in particular their scales which linearly enter the cross section formula (1).

We made two cross checks with VELO detector, first, by comparing the luminous region positions measured in two scans, and second, we made a dedicated mini-scan in October when we moved the beams with constant separation.

In case of identical beams the luminous region is centered at the middle between them, otherwise it is shifted towards the narrower beam. The deviation from the middle is a function of the beam separation which we denote by $\Delta \vec{r}_{\text{Lum}}(\Delta x, \Delta y)$. When the beams are moved symmetrically in the first scan, the middle is always at zero, so the deviation coincides with the luminous region center, $\Delta \vec{r}_{\text{Lum}}(\Delta x, \Delta y) = \vec{R}_{\text{Lum}}^I$. Here I stands for the first scan and ‘‘Lum’’ is for the luminous center. When only the first or the second beam is moved by $\vec{R}_{b1,2}^{II}$ in the second scan, the middle between the beams is at $\vec{R}_{b1,2}^{II}/2$ and $\Delta \vec{r}_{\text{Lum}}(\Delta x, \Delta y) = \vec{R}_{\text{Lum}}^{II} - \vec{R}_{b1,2}^{II}/2$. Since $\Delta \vec{r}_{\text{Lum}}(\Delta x, \Delta y)$ should be the same function in both scans, we have a constraint $\vec{R}_{b1,2}^{II}/2 = \vec{R}_{\text{Lum}}^{II} - \vec{R}_{\text{Lum}}^I$ independently of the beam shapes. The luminous region centers \vec{R}_{Lum}^I and $\vec{R}_{\text{Lum}}^{II}$ can be precisely measured in VELO. Its dependence on the beam separation in April is shown in Fig. 12. Blue solid lines (red dashed) is for the first (second) scan. One can see that the former is not linear as it should be for single Gaussian beams. At the scan ends the center is closer to the first beam meaning that the second is broader.

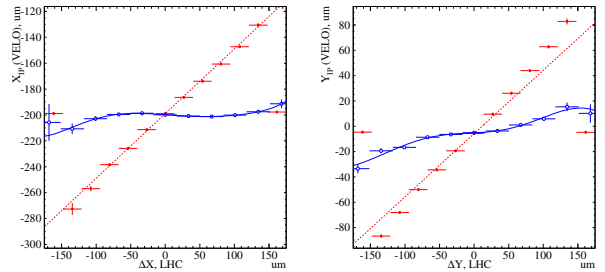


Figure 12: The luminous region center measured in VELO versus the beam separation Δx (left) or Δy (right), in April. The first (second) scan is shown by blue open (red filled) points. The curves are the fit by 7th order polynomial. Horizontal bars represent not the errors but the bin width.

The difference between the curves for the second and for the first scan, multiplied by two, is shown in Fig. 13. Inde-

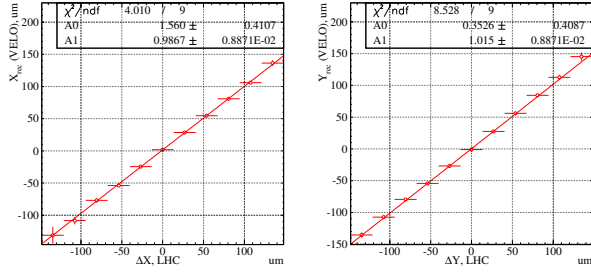


Figure 13: Difference between two curves in Fig. 12 multiplied by two. Results of the fit by a straight line are shown in the top right corner.

pendently of the bunch shapes it should be linear. The fit returns the slopes compatible with unity within $-1.3 \pm 0.9\%$ and $1.5 \pm 0.9\%$ for Δx and Δy , respectively. In spite of opposite signs of Δx and Δy corrections, we conservatively assigned 2% systematic error for the length scale calibration in April. Note, also that in Δx there is a shift by $1.5 \mu\text{m}$ at zero between the two scans.

Dedicated length scale calibration scan in October

In October we used another calibration method. Beams have been moved in 5 equidistant steps in Δx and Δy but the separation between them was kept constant. The luminous center movement is shown in Fig. 14. Red points above flat intervals distinguish periods with fixed beam positions which we used in the following analysis. They are shifted upwards only for illustration purposes. During the scan along x the beam separation was $(\Delta x, \Delta y) = (-80 \mu\text{m}, 0)$. Here $80 \mu\text{m}$ is approximately one sigma of van der Meer luminosity dependence on $\Delta x = x_1 - x_2$. This separation was chosen to maximize the derivative $dL/d\Delta x$, i.e. the luminosity sensitivity to possible difference in the two beam scales. If e.g. the first beam moves slightly faster than the second, the separation Δx gets smaller and the effect can be visible in the increase of the luminosity. The same separation $\Delta y = 80 \mu\text{m}$ was chosen in the y scan.

Difference between beam scales. The luminosity behaviour during the scans is shown in Fig. 15. As one can see it is not constant. This may be attributed to the different scales of two beams. Mote specifically, we assumed that the real positions of the beams $x_{1,2}$ can be obtained from the predicted numbers $x_{1,2}^0$ by applying a correction

$$x_{1,2} = (1 \pm \epsilon_x/2) \cdot x_{1,2}^0, \quad (2)$$

and the same for $y_{1,2}$. Assuming a Gaussian shape of van der Meer luminosity dependence on Δx , with sigma σ , we get in this case

$$\frac{1}{L} \cdot \frac{dL}{d(x_1 + x_2)/2} = -\epsilon_x \frac{\Delta}{\sigma^2}. \quad (3)$$

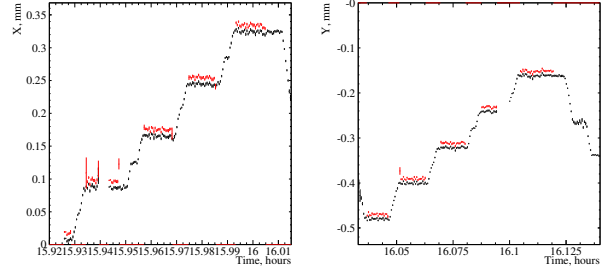


Figure 14: Evolution of the luminous center in x (left) and in y (right) during length scale calibration scans in October. Red points above flat intervals distinguish periods used in the following analysis. They are shifted upwards only for illustration purposes. During the first (second) scan the beams were moved in 5 equidistant steps of $80 \mu\text{m}$ along x (y) with the constant separation $\Delta x = 80 \mu\text{m}$, $\Delta y = 0$ ($0, 80 \mu\text{m}$).

Here $\Delta = 80 \mu\text{m}$ is the fixed beam separation. From the slopes in Fig. 15 we obtain $\epsilon_x = 2.4\%$ and $\epsilon_y = -1.9\%$. The luminosity in different bunches changes coherently, as shown in Fig. 16.

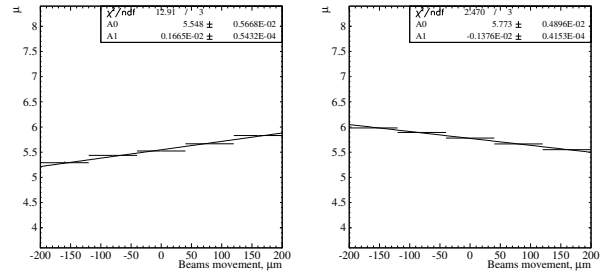


Figure 15: Average number of interactions summed over 12 colliding bunches versus the luminous center during length scale scans in x (left) and in y (right) in October. The fit by a straight line is overlaid, the fit results are given in the top right corner.

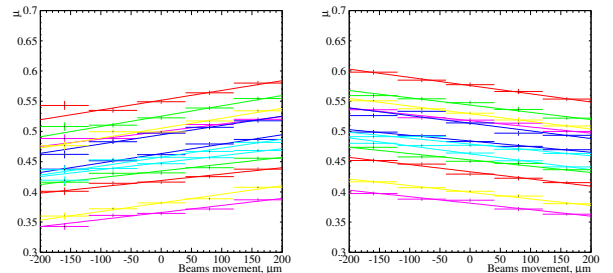


Figure 16: The same as in Fig. 15 but separately for different bunches.

Since $\Delta x = (x_1^0 - x_2^0) + \epsilon \cdot (x_1^0 + x_2^0)/2$, it depends on the

middle point between the beams $(x_1^0 + x_2^0)/2$. In the first scan it is always at zero, therefore no correction is needed. During the second scan this point moved $0 \rightarrow 355.9 \mu\text{m} \rightarrow 0$. Therefore a correction of Δx values in Fig. 7 is required. The central point should be shifted to the right (left) for the x (y) scan. The left (right) side is thus stretched and the opposite side is shrunk. The corrected curves are shown in Fig. 17. One can see, that the shift between the scans is reduced in y , but appears in x , so that the discrepancy can not be fully explained just by a linear correction.

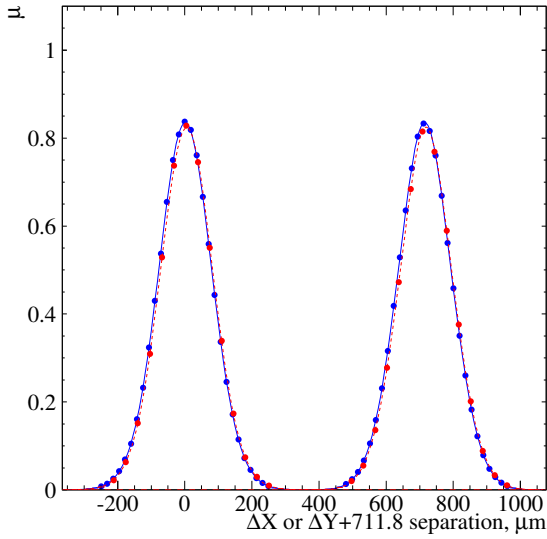


Figure 17: The same plots as in Fig. 7 but with $\epsilon_{x,y}$ correction discussed in the text. Δx and Δy curves are stacked one after the other for illustration purposes.

Stretching and shrinking the second scan curves influences the integrals and the resulting cross sections very little. The latter changes in average only by 0.1%, which we include into a systematic error. In fact, in Table 4 and in Fig. 9 the numbers are given after the correction.

Cross check of a common beam scale. In case of parallel translation of both beams, the luminous center should follow the beam positions regardless of the bunch shapes. Since it is approximately at $(x_1 + x_2)/2 = (x_1^0 + x_2^0)/2$ and similar for y , the corrections due to $\epsilon_{x,y}$ are negligible. The luminous center can be measured with VELO. This provides a precise cross check of the common beam scales $(x_1^0 + x_2^0)/2$ and $(y_1^0 + y_2^0)/2$.

The result is shown in Fig. 18. The LHC and VELO scales agree within $-0.97 \pm 0.17\%$ and $-0.33 \pm 0.15\%$ in x and y , respectively. For the cross section determination we took a more precise VELO scale and multiplied the values from Table 4 by $(1 - 0.0097) \cdot (1 - 0.0033)$. In addition, we conservatively assigned 1% systematic error due to the common scale uncertainty.

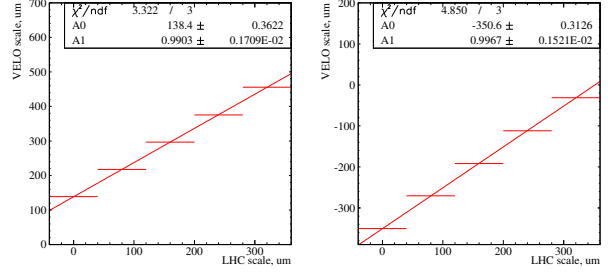


Figure 18: Luminous center reconstructed in VELO versus the position predicted from LHC magnets. The horizontal bars represent the bin widths, not the errors. The points are fit to a linear function. The slope, shown in the top right corner, calibrates the common beam scale.

x - y coupling

LHC ring tilt. Van der Meer formula (1) is valid only if the particle distributions in x and in y are independent. To check this statement we measured the movement of the luminous center along y during length scale scan in x and vice versa, see Fig. 19. The slope is compatible within errors with the expected at LHCb 13 mrad tilt of the LHC ring [12] with respect to vertical and horizontal axes of VELO. Note, that due to this tilt the LHC and VELO scales differ by $1 - \cos(13 \text{ mrad}) = 0.84 \cdot 10^{-4}$ both in x and y . The corresponding correction to the cross section is negligible.

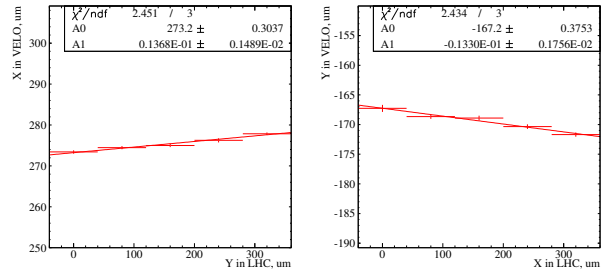


Figure 19: Luminous center position in x during length scale scan in y (left) and vice versa (right). The points are fit to a linear function. The slope, shown in the top right corner, is compatible with the expected 13 mrad tilt of LHC ring at LHCb.

x - y independence of the luminous region. In addition we checked x - y independence of the vertex distribution. To increase statistics we used data collected in the same LHC fill 1422 after van der Meer scan at LHCb when the beams collided head-on. Fig. 20 shows RMS spread of vertexes in y in different slices in x and vice versa. From the first glance there is a big x - y correlation. However, the same plot for the sample of vertexes with > 40 tracks and thus better resolution, is much more flat, see Fig. 21.

Clearly, the x tails of the luminous region contain more poorly measured vertexes, which produce larger RMS in y . This explains Fig. 20, x - y correlation appears via a cross correlation with the vertex resolution.

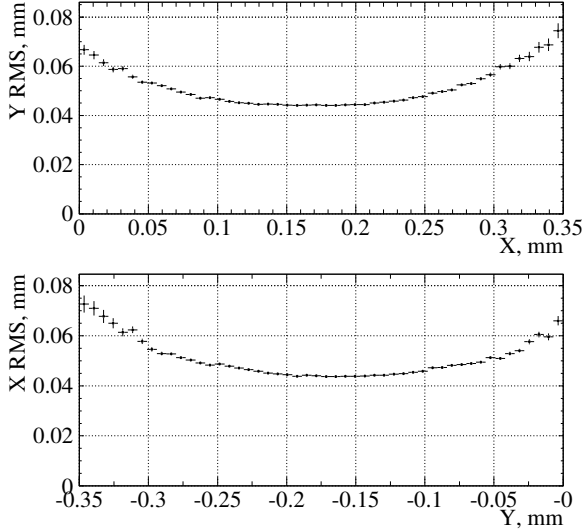


Figure 20: Luminous center RMS in y in different x slices (top) and vice versa (bottom). The data was collected after LHCb van der Meer scan, with head-on beams.

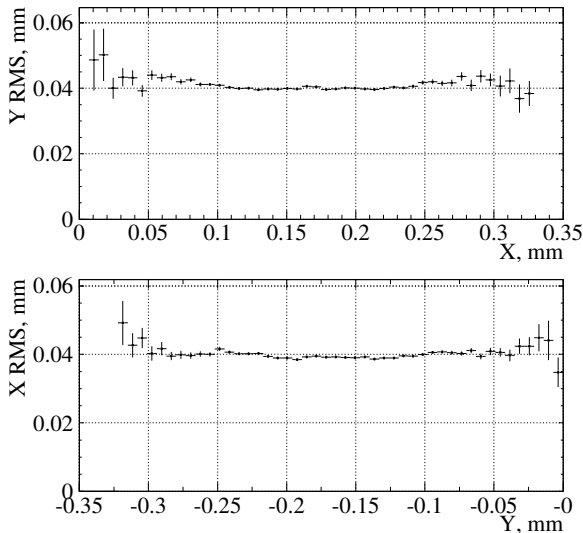


Figure 21: The same as in Fig. 20 but only for vertexes with > 40 tracks.

Fig. 22 shows the x - y profile of the luminous region. There is a slope of 79 mrad. Its origin is not understood. The corresponding x - z and y - z profiles are given in Fig. 23. The slopes of -92 and 44 μ rad are due to the known fact that the middle line between LHC beams is inclined from the z

axis. This was observed with beam gas events, the inclination varies slightly from fill to fill. Taking into account these x and y cross correlations with z and also the known 13 mrad tilt of LHC ring, one can calculate the residual x - y correlation slope, which was found to be 77 mrad.

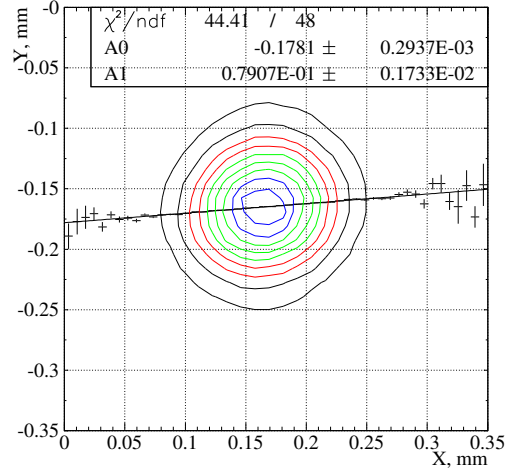


Figure 22: Contours of x - y luminous region profile. The points represent y -coordinates of the luminous center in different x slices. They are fit with the linear function. The slope (A1) is given in the top right corner.

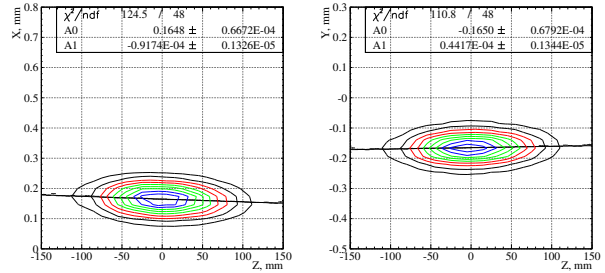


Figure 23: Similar to Fig. 22 but in x - z and y - z projections.

If the beam profiles are two-dimensional Gaussians of the general type with a non-zero correlation between x and y , the cross section formula should be corrected. The details are given in Appendix. We assumed that the correlation coefficients of two beams were similar and therefore close to the measured correlation in the luminous distribution $\xi = 0.077$. In this case the cross section correction is $\xi^2/2 = 0.3\%$. We did not apply this correction, but included 0.3% as a systematic error.

Ghost charge in LHC ring

There is a small fraction of “ghost” protons contained in not nominal LHC RF buckets. This is discussed in [8], [9]. Their contribution to the total LHC beam current should be subtracted.

Ghost charge in not nominal bunches. With the dedicated trigger in LHCb we were able to measure the rates of beam-gas events produced by ghost and nominal protons, and to determine the ghost fraction from their ratio. The results for the October and April fills are summarized in Table 6. LHCb trigger efficiency is timing dependent, it is optimized for the interactions in the nominal RF buckets. For the satellite buckets the efficiency drops as it is shown in Fig. 24. This was measured in van der Meer October fill by shifting LHCb clock by 5, 10 and 12.5 nsec and by comparing the total beam-gas rates in the nominal crossings. Since the RF bucket number within 25 nsec bunch is not measured in LHCb, this uncertainty through the efficiency dependence introduces some systematics in ghost charge measurement. We considered two extreme cases, when all ghost charge was contained at the nominal RF positions and thus the timing efficiency was 100%, and when the efficiency was at the average level for 5, 10 and 12.5 nsec points. The latter should be below the efficiency averaged over *all* RF buckets. We took the average between these two extremes as an approximation of the efficiency and half of the difference between them as an error. We also fit four available points at 0, 5, 10 and 12.5 nsec to the periodic function $R_{\max} \cdot (\epsilon + (1 - \epsilon) \cdot \cos(2\pi\Delta t/25 \text{ nsec}))$. Here R_{\max} is the maximal rate at zero and ϵ estimates the average efficiency due to timing for the random distribution of the ghost charges in RF buckets. The obtained ϵ values are close to our efficiency central values, as it can be seen from Table 6. Finally, the cross section correction due to the ghost charge is $\frac{0.12 \pm 0.06}{0.86 \pm 0.14} + \frac{0.00 \pm 0.03}{0.84 \pm 0.16} = 0.14 \pm 0.08\%$ in April and $\frac{0.20 \pm 0.02}{0.86 \pm 0.14} + \frac{0.36 \pm 0.03}{0.84 \pm 0.16} = 0.66 \pm 0.10\%$ in October.

Table 6: From top to bottom: total ghost charge fraction outside nominal bunches in October. Fractions localized in ± 3 bunches around the nominal positions. The same two lines for April. Ratio of the average rate measured with 5, 10, 12.5 nsec time shifts and the rate at zero. Estimation of the efficiency due to timing. Average efficiency from the fit to the sum of a cosine and a constant.

	Beam 1	Beam 2
Fraction in Oct., % (in ± 3 BX)	0.20 ± 0.02 (0.12 ± 0.01)	0.36 ± 0.03 (0.25 ± 0.02)
Fraction in Apr., % (in ± 3 BX)	0.12 ± 0.06 (0.12 ± 0.06)	0.00 ± 0.03 (0.00 ± 0.03)
5, 10, 12.5 ns avr.	0.73	0.67
Efficiency	0.86 ± 0.14	0.84 ± 0.16
ϵ	0.83 ± 0.04	0.78 ± 0.04

Ghost charge in the satellite RF buckets in the nominal bunches. It is known that there may be a ghost charge in the satellite RF buckets in the nominal bunches. Usually it may be present in $\pm 2, 4, \dots$ buckets around the nominal position which is attributed to the SPS frequency of

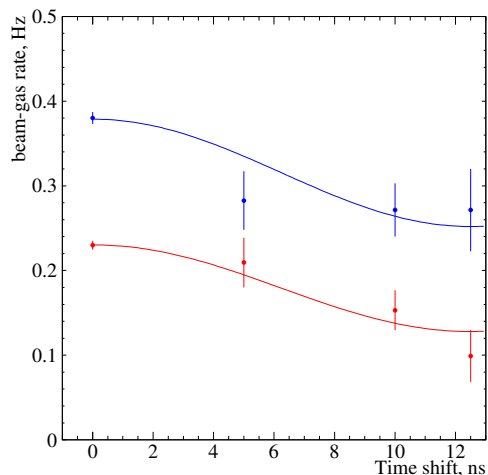


Figure 24: Beam-gas rate proportional to the trigger efficiency versus the time shift of the interaction from LHCb clock. The curve is the fit to the function $R_{\max} \cdot (\epsilon + (1 - \epsilon) \cdot \cos(2\pi\Delta t/25 \text{ nsec}))$, which returns the timing trigger efficiency for the random distribution of ghost charge $\epsilon = 0.83 \pm 0.04$ and 0.78 ± 0.04 for the first and the second beam, respectively.

200 MHz [8], [9]. Due to LHCb crossing angle of $170 \mu\text{rad}$ in October, ± 2 and the nominal buckets are separated in x and can not collide if the beams are head-on. However, as it is schematically illustrated in Fig. 25, when the beams are separated in x by about $225 \mu\text{m}$ the collisions are possible at $z = \pm 75 \text{ cm}$. The z distribution of vertexes accumulated with the minimum bias trigger in October is shown in logarithmic scale in Fig. 26. To estimate the fraction of the ghost charge, we counted a number of vertexes at $z = 0, \pm 75 \text{ cm}$ versus the separation x , see Fig. 27. Since the rate of the minimum bias events was biased by the trigger rate limiter, we took vertex distributions with the weights determined from the sample of nano-events taken with random trigger. Assuming similar efficiencies and distribution of particles in the nominal and the satellite ± 2 RF buckets, the fraction of the charge in the latter is determined to be 0.1%. We did not correct for this effect but assigned a systematic error of 0.1%.

Reproducibility of the luminosity at the nominal beam positions

As it can be seen from Fig. 5, when the beams were brought to their nominal positions, the luminosity not always returned to the expected value. $\chi^2/\text{ndf} = 40/12$, so the non reproducibility can not be fully attributed to statistical fluctuations and some systematic error should be present. It is origin is not understood but the effect may be similar to the non reproducibility of the beam positions visible from the shift of two scan curves in Figs. 7, 8 and 17.

We denote sigma of the statistical fluctuations by σ_{stat}

and assume that the extra systematic fluctuations may also be described by a Gaussian with sigma σ_{syst} . A luminosity measurement time, an accumulated statistics and thus σ_{stat} at different points were the same. Since the statistical error alone gives $\chi^2/\text{ndf} = \sum_i (\Delta_i)^2 / \sigma_{\text{stat}}^2 / \text{ndf} = 40/12$, to bring it to unity one should add the systematics σ_{syst} determined from $(\sigma_{\text{syst}}^2 + \sigma_{\text{stat}}^2) / \sigma_{\text{stat}}^2 = 40/12$. The relative statistical error is $\sigma_{\text{stat}} = 0.00209 / 0.8356 = 0.25\%$, so that $\sigma_{\text{syst}} = \sigma_{\text{stat}} \sqrt{39.84/12 - 1} = 0.38\%$. The absolute scale of μ measurement enters the cross section formula (1) twice in the numerator and once in the denominator, so the overall dependence is linear. Therefore we assigned an extra systematic error of 0.4% to the cross section measurement.

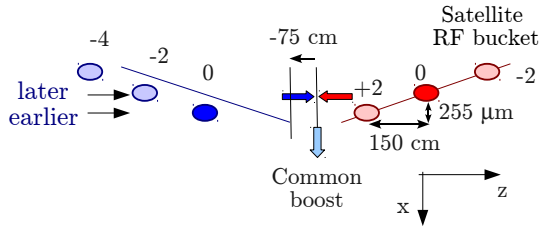


Figure 25: Collision of protons from the nominal and ± 2 satellite RF buckets in van der Meer scan.

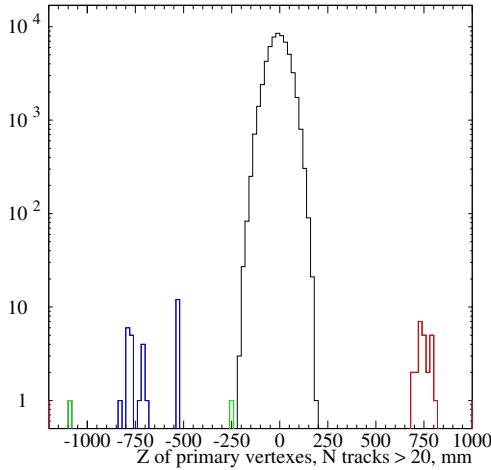


Figure 26: z distribution of vertexes in the minimum bias sample in the first Δx scan. Vertexes at ± 75 cm are due to interactions of protons in the nominal and ± 2 satellite RF buckets.

BEAM IMAGING DURING VAN DER MEER SCAN

During van der Meer scan the transverse beam images can be reconstructed [11]. One should accumulate transverse vertex distributions visible from the beam center and unfold them with the transverse vertex resolution. This

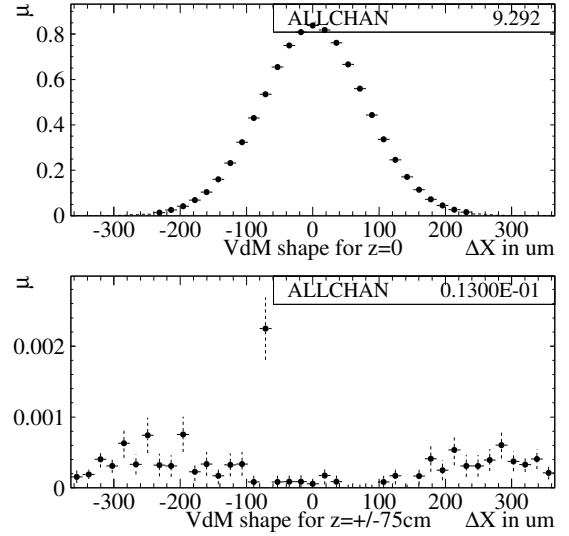


Figure 27: Average number of interactions μ at $z = 0$ (top) and $z = \pm 75$ cm (bottom) versus the beam separation Δx corrected for the trigger bias of the minimum bias sample. It is assumed that the efficiencies and the distribution of particles in the nominal and the satellite \pm RF buckets are the same.

should give the beam image in its transverse plane for arbitrary beam shapes. The approach is complementary to the beam-gas method.

The beam imaging was used to cross check the widths of van der Meer luminosity versus separation curves in October data. The x and y VELO vertex resolution was determined from data in the following way. N vertex tracks were randomly split into two equal halves to form two independent vertexes. Their separation divided by $\sqrt{2}$ gave a resolution estimate for a vertex with $N/2$ tracks. The resolution was then parameterized with the function $\sigma/N^\alpha + \delta$ with σ , α and δ parameters and their errors given in Table 7. For the beam imaging we used only tracks with $N > 10$. The average resolution function was reconstructed for the N -distribution observed in data. This was done for the central values of σ , α and δ parameters, and for the values shifted by one sigma to the left or to the right to simultaneously minimize or maximize the resolution. To simplify deconvolution, the obtained resolution functions, shown in Fig. 28, were approximated as Gaussians. The beam images were also approximated as Gaussians, the corresponding widths after unfolding are shown in fig. 29. The beam transverse planes were defined using the known crossing angle of $170 \mu\text{rad}$ and the measured inclination of the luminous ellipsoid from the z axis. As it is discussed in [11], the luminosity depends on the beam profiles along x , while the beam imaging gives the widths $\sigma_{x1,2}$ of the profiles perpendicular to the beams. Due to the crossing angle $\alpha = 170 \mu\text{rad}$, the former is broader due to

a contribution from the z -length of the bunch. To correct for this effect we assumed that the bunches of two beams were of the same length and determined it from the width of the luminous region as $\sqrt{2}\sigma_{\text{Lum}}^z$. The widths of van der Meer luminosity versus separation curves finally can be obtained as $\sqrt{\sigma_{x1}^2 + \sigma_{x2}^2 + 4(\sigma_{\text{Lum}}^z)^2\alpha^2}$, their ratio with the measured values is show in Fig. 30. The points (band) corresponds to the central values (one sigma change) of the vertex resolution parameters. As one can see the method is very sensitive, the band width is about 1.2% and the RMS spread of the points is 0.5-0.8%. Assuming equal weights of the points, they were fit to a constant. The obtained average ratio is compatible with unity within 0.4-0.6%. This proves both the widths of van der Meer luminosity versus separation curves which effectively enter the cross section formula (1), and the vertex resolution at LHCb which is important in the beam-gas luminosity determination.

Table 7: VELO vertex resolution parameters and their errors.

	x	y
$\sigma, \mu\text{m}$	0.2148 ± 0.01962	0.2023 ± 0.01806
α	1.023 ± 0.05375	1.008 ± 0.05257
$\delta, \times 10^{-3} \mu\text{m}$	5.463 ± 0.675	4.875 ± 0.6451

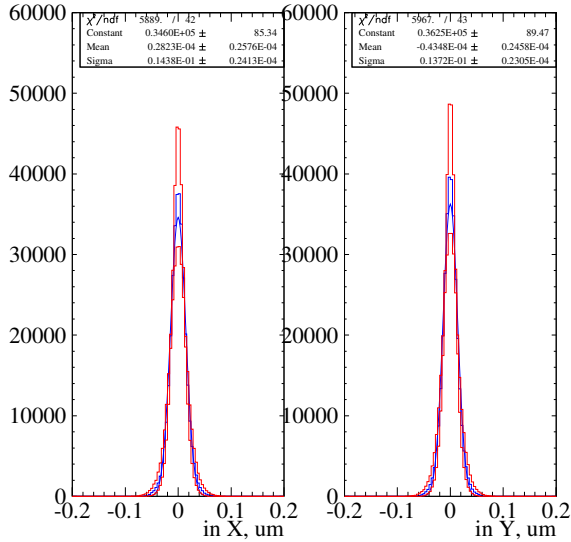


Figure 28: VELO resolution functions obtained for the observed distribution of the number of vertex tracks N . Middle curve corresponds to the central values of σ , α and δ resolution parameters discussed in the text. Narrower and wider curves are obtained for the parameters simultaneously shifted by one sigma in the direction minimizing or maximizing the resolution.

The width of van der Meer Δx curve was also checked by measuring the z -movement of the luminous center dur-

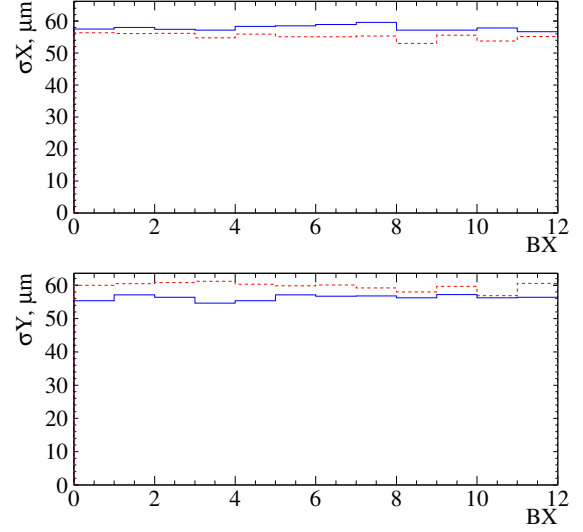


Figure 29: Gaussian widths of the reconstructed beam profiles after unfolding with VELO resolution in the plane transverse to the beam in different bunch crossings. Solid blue (dashed red) curves are for the first (second) beam.

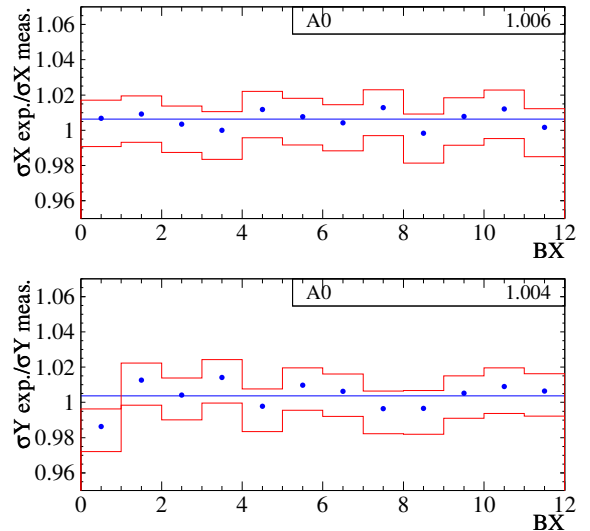


Figure 30: Ratio of expected from the reconstructed beam images and measured widths of van der Meer luminosity versus Δx (top) or Δy (bottom) curves in different bunch crossings. The band corresponds to one sigma variation of the resolution parameters. The points are fit to a constant, the result is shown in the top right corner.

ing the first scan in x . It is shown in Fig. 31. According to [13], in case of identical beams the slope should be equal to

$$\frac{\delta z}{\Delta x} = \frac{\sin 2\alpha}{4} \frac{\sigma_z^2 + \sigma_x^2}{\sigma_x^2 \cos^2 \alpha + \sigma_z^2 \sin^2 \alpha},$$

where $\sigma_{x,z}$ are the transverse and longitudinal beam widths, δz is the induced z -shift of the luminous center. We approximate again σ_z as $\sqrt{2}\sigma_{\text{Lum}}^z$. Since VELO resolution in z is much better than $\sigma_{\text{Lum}}^z = 52.0 \pm 0.3$ mm, it is neglected. Using the slope from Fig. 31 one gets the expected width of van der Meer Δx curve $\sigma_x^{\text{VDM}} = \sqrt{2}\sigma_x = 78 \mu\text{m}$ in agreement with the measured value of $80 \mu\text{m}$.

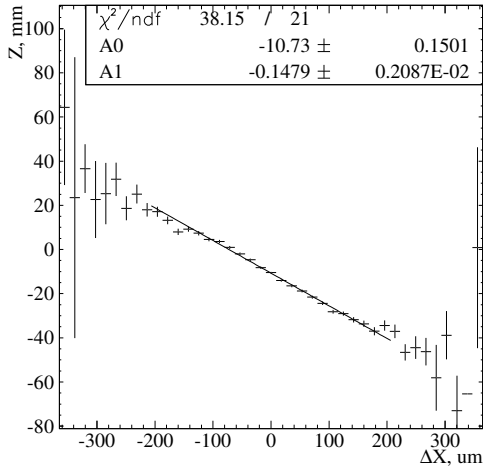


Figure 31: Movement of the luminous center in z during the first scan in Δx . The slope (A1) is given in the top right corner.

CONCLUSIONS

The absolute calibration of luminosity was performed in LHCb in 2010 using two van der Meer scans and the beam-gas method. They gave similar accuracy dominated by the bunch intensity uncertainties. Here we concentrate on the results of van der Meer scans in April and in October. The visible cross section is measured for events having at least two VELO tracks in R - Z projection. The fraction of such events in randomly triggered sample is continuously monitored during LHCb data taking. This allows to extrapolate our measurements to the whole LHCb statistics.

The cross section results are given in Table 8¹. They are all consistent with each other. For the final LHCb luminosity calibration we averaged the cross sections measured in the first scan in October and in the beam-gas method. During the second scan in October the beam movements were not continuous, so the results might suffer from the hysteresis effects. Both in April and in October measurements

the difference between the scans was included as a systematic error. The complete list of errors is given in Tables 9 and 10.

Table 8: Cross section of the interaction producing at least two VELO tracks in R - Z projection, measured in two van der Meer scans in April and in October and obtained with the beam-gas method. Cross sections from the first October scan and from the beam-gas analysis were averaged for the final LHCb luminosity calibration in 2010.

	$\sigma(RZ)$, mb	rel. error, %
April	59.6, 57.0	7.5
October	<u>58.4</u> , 57.1	3.6
Beam-gas method	<u>60.8</u>	4.5

Table 9: Summary of cross section relative errors for van der Meer scan in April. Last column contains correction to the cross sections listed in Table 5.

Source	error, %	corr., %
$I_1 \times I_2$	5.6	
Diff. btw. scans	4.4	
Length scale	2	
Stat. error	0.9	
RZVelo stability	0.5	
Ghosts in other BX	0.08	+0.14
Ghosts in ± 2 RF	neglig.	
$I_1 \times I_2$ drop	neglig.	
Emittance growth	neglig.	
Total	7.5	

In the future van der Meer scans in 2011 the DC BCT accuracy should be improved. Note, that Fast BCT did not contribute to October systematics since we determined the Fast BCT offsets directly from the fit, and therefore the statistical error 0.09% already includes this contribution. With significantly improved BCT scale uncertainty, the error will be dominated by non reproducibility of the scans. This is not fully understood but may be attributed to the uncertainties in the beam positions during the scan. Note, that there is always a very good agreement between different bunches, so the problem should be in the beam as a whole.

To push the error further down one may think of either the precise measurement of the beam positions or of precisely controllable beam movements, which should not necessarily be linear but may be more complicated, e.g. sinusoidal.

To study systematic effects further it will be advantageous to have as different bunches as possible. Difference in bunch intensities may provide better sensitivity to the Fast BCT offset measurement. Comparing the bunches with high and low intensities allows to estimate possible beam-beam effects. Broad and narrow bunches could help reveal systematics which depends on the bunch shapes.

¹The beam-gas results is an update of [6]

Table 10: Summary of cross section relative errors for van der Meer scan in October. Last column contains corrections to the cross section central values from Table 4 with Fast BCT intensities.

Source	error, %	corr., %
BCT scale	2.7	
Diff. btw. scans	2.1	
Length scale	1	-1.3
RZVelo stability	0.5	
Working point stability	0.4	
Non-diag. xy cov.matrix	0.3	
Ghosts in other BX	0.15	+0.66
Ghosts in ± 2 RF	0.1	
Beam scale difference	0.1	
Stat. error	0.09	
$I_1 \times I_2$ drop	neglig.	
Emittance growth	neglig.	
Total	3.6	

In LHCb it is also very advantageous to perform beam-gas measurements during van der Meer LHC fill.

APPENDIX

Here we calculate the cross section correction in case when the beam profiles are two-dimensional Gaussians of the general type with non zero x - y correlation term,

$$\rho_{1,2}(r) = \frac{1}{\sqrt{|2\pi\Sigma_{1,2}|}} \exp\left(-\frac{1}{2}(r - r_{1,2})^T \Sigma_{1,2}^{-1}(r - r_{1,2})\right).$$

Here

$$\Sigma_{1,2} = \begin{bmatrix} \Sigma_{x1}^2 & \xi_{1,2}\Sigma_{x1,2}\Sigma_{y1,2} \\ \xi_{1,2}\Sigma_{x1,2}\Sigma_{y1,2} & \Sigma_{y1,2}^2 \end{bmatrix}, \quad r_{1,2} = \begin{bmatrix} x_{1,2} \\ y_{1,2} \end{bmatrix}$$

are the covariance matrices and Gaussian centers. $|2\pi\Sigma_{1,2}|$ denote the determinants of the matrices $2\pi\Sigma_{1,2}$. It may be shown that the overlap integral $\rho = \int \rho_1(r)\rho_2(r) d^2r$ is

$$\rho(\Delta r) = \frac{1}{\sqrt{|2\pi\Sigma_0|}} \exp\left(-\frac{1}{2}\Delta r^T \Sigma_0^{-1}\Delta r\right),$$

where

$$\Delta r = r_1 - r_2 = \begin{bmatrix} \Delta x \\ \Delta y \end{bmatrix},$$

$$\Sigma_0 = \Sigma_1 \frac{1}{\Sigma_1 + \Sigma_2} \Sigma_2 = \begin{bmatrix} \Sigma_{x0}^2 & \xi_0 \Sigma_{x0} \Sigma_{y0} \\ \xi_0 \Sigma_{x0} \Sigma_{y0} & \Sigma_{y0}^2 \end{bmatrix}$$

are the beam separations and the two-dimensional analog of the width of van der Meer luminosity versus separation function. The analog of the luminous width is $\Sigma = \Sigma_1 + \Sigma_2$. If the Δx - Δy correlation coefficient is not zero, $\xi_0 \neq 0$, the cross section formula (1) should be modified. Instead of Δr it is convenient to use the normalized coordinates

$$\chi = \begin{bmatrix} \chi_x \\ \chi_y \end{bmatrix} = \begin{bmatrix} \Delta x / \Sigma_{x0} \\ \Delta y / \Sigma_{y0} \end{bmatrix}.$$

Since

$$\Sigma_0^{-1} = \frac{1}{1 - \xi_0^2} \begin{bmatrix} 1/\Sigma_{x0}^2 & -\xi_0/\Sigma_{x0}/\Sigma_{y0} \\ -\xi_0/\Sigma_{x0}/\Sigma_{y0} & 1/\Sigma_{y0}^2 \end{bmatrix}$$

we have then

$$\Delta r^T \Sigma_0^{-1} \Delta r = \chi^T \tilde{\Sigma}_0^{-1} \chi$$

where

$$\tilde{\Sigma}_0 = \begin{bmatrix} 1 & \xi_0 \\ \xi_0 & 1 \end{bmatrix}$$

and

$$\rho(\chi) = \frac{1}{2\pi\Sigma_{x0}\Sigma_{y0}\sqrt{1 - \xi_0^2}} \exp\left(-\frac{\chi_x^2 - 2\xi_0\chi_x\chi_y + \chi_y^2}{2(1 - \xi_0^2)}\right).$$

We'll denote the cross section calculated from Eq. (1) by σ_{fact} since it is valid only in the case of x - y factorization. The general formula is

$$\sigma_{\text{true}} = \frac{\int \mu(\Delta x, \Delta y) d\Delta x d\Delta y}{N_1 N_2 \cos \alpha},$$

and the required correction

$$\frac{\sigma_{\text{true}}}{\sigma_{\text{fact}}} = \frac{\mu(\Delta x_0, \Delta y_0) \cdot \int \mu(\Delta x, \Delta y) d\Delta x d\Delta y}{\int \mu(\Delta x, \Delta y_0) d\Delta x \cdot \int \mu(\Delta x_0, \Delta y) d\Delta y}.$$

With the non-diagonal covariance matrix, if

$$\mu(\Delta x_0, \Delta y_0) \propto \exp\left(-\frac{\chi_{x0}^2 - 2\xi_0\chi_{x0}\chi_{y0} + \chi_{y0}^2}{2(1 - \xi_0^2)}\right),$$

then with the same proportionality factor

$$\int \mu(\Delta x, \Delta y) d\Delta x d\Delta y \propto 2\pi\Sigma_x\Sigma_y\sqrt{1 - \xi_0^2},$$

$$\int \mu d\Delta_i \propto \int \exp\left(-\frac{(\chi_i - \xi_0\chi_{j0})^2 + (1 - \xi_0^2)\chi_{j0}^2}{2(1 - \xi_0^2)}\right) \times \\ \times d(\Sigma_i\chi_i) = \sqrt{2\pi(1 - \xi_0^2)}\Sigma_i \exp\left(-\frac{\chi_{j0}^2}{2}\right),$$

where $i = x, y$ and (χ_{x0}, χ_{y0}) denote the normalized coordinates of the crossing point $(\Delta x_0/\Sigma_{x0}, \Delta y_0/\Sigma_{y0})$. Therefore, the measured widths of van der Meer μ versus Δ_i functions are

$$\Sigma_{x,y}^{\text{meas}} = \Sigma_{x,y}\sqrt{1 - \xi_0^2}.$$

Finally,

$$\frac{\sigma_{\text{fact}}}{\sigma_{\text{true}}} = \sqrt{1 - \xi_0^2} \exp\left(-\frac{\xi_0\chi_{x0}\chi_{y0}}{1 - \xi_0^2} + \frac{\xi_0^2(\chi_{x0}^2 + \chi_{y0}^2)}{2(1 - \xi_0^2)}\right) \\ \approx 1 - \frac{\xi_0^2}{2} - \xi_0\chi_{x0}\chi_{y0}$$

The exponent term coming from $\mu(\Delta x_0, \Delta y_0)$, gives a correction only if the crossing point (χ_{x0}, χ_{y0}) is not centered at zero. For the October LHCb scan it is negligible. The coefficient ξ_0 is determined by the covariance matrices of both beams $\Sigma_{1,2}$. It is impossible to obtain it only from the measurable matrix $\Sigma = \Sigma_1 + \Sigma_2$ of the luminous region. However, for the systematic error estimation we assumed that ξ_0 is at the same level as the correlation coefficient in Σ (0.077), which is the case e.g. for the similar beam covariance matrices.

REFERENCES

- [1] H. Dijkstra and O. Schneider, "Online and offline monitoring of the relative luminosity at LHCb", LHCb note 2008-034.
- [2] V. Balagura, "Analysis methods for luminosity data", LHCb note LHCb-INT-2009-001.
- [3] M. Ferro-Luzzi, Nucl. Instrum. and Methods A 553 (2005) 388.
- [4] R. Aaij *et al.*, LHCb collaboration, Phys. Lett. B 693 (2010) 69.
- [5] R. Aaij *et al.*, LHCb collaboration, Phys. Lett. B 694 (2010) 209.
- [6] P.Hopchev, "LHCb beam-gas imaging results", contribution to this LHC Lumi Days workshop, CERN (2011).
- [7] Van der Meer, "Calibration of the Effective Beam Height in the ISR", internal CERN report, ISR-PO/68-31 (1968).
- [8] G. Anders *et al.*, "LHC Bunch Current Normalisation for the April-May 2010 Luminosity Calibration Measurements", CERN-ATS-Note-2011-004 PERF.
- [9] G. Anders *et al.*, "LHC Bunch Current Normalisation for the October 2010 Luminosity Calibration Measurements", CERN-ATS-Note-2011-016 PERF.
- [10] J.J. Gras, M Ludwig and P. Odier, "The 2010 LHC DC BCT measurement system and its main sources of uncertainties", CERN-LHC-Project-Note-432;
D. Belohrad, J.J. Gras, M. Ludwig, "The 2010 LHC ring Fast BCT measurement system and its main sources of uncertainties", CERN-LHC-Project-Note-433;
D. Belohrad *et al.*, "Commissioning and First Performance of the LHC Beam Current Measurement Systems", 1st IPAC, Kyoto, Japan, 23 - 28 May 2010.
- [11] V. Balagura, "Notes on van der Meer Scan for Absolute Luminosity Measurement", arXiv:1103.1129 [physics.ins-det], submitted to Nucl. Instrum. and Methods A.
- [12] C. Lasseur *et al.*, "Gomtrie Du LHC : Points Caractristiques, Formules De Transformation", CERN-LHC-Project-Note-95 (1997).
- [13] M. Ferro-Luzzi, private communication.